Quantifying the 3D structure and function of porosity and pore space in natural sediment flocs

T. J. Lawrence[1,4] · S. J. Carr[1,2] · J. A. T. Wheatland[1,5] · A. J. Manning[3] · K. L. Spencer[1]

Abstract

Purpose Flocculated cohesive suspended sediments (flocs) play an important role in all aquatic environments, facilitating the transport and deposition of sediment and associated contaminants with consequences for aquatic health, material fluxes, and morphological evolution. Accurate modelling of the transport and behaviour of these sediments is critical for a variety of activities including fisheries, aquaculture, shipping, and waste and pollution management and this requires accurate measurement of the physical properties of flocs including porosity.

Methods Despite the importance of understanding floc porosity, measurement approaches are indirect or inferential. Here, using μCT, a novel processing and analysis protocol, we directly quantify porosity in natural sediment flocs. For the first time, the complexity of floc pore spaces is observed in 3-dimensions, enabling the identification and quantification of important pore space and pore network characteristics, namely 3D pore diameter, volume, shape, tortuosity, and connectivity.

Results We report on the complexity of floc pore space and differentiate effective and isolated pore space enabling new understanding of the hydraulic functioning of floc porosity. We demonstrate that current methodological approaches are overestimating floc porosity by c. 30%.

Conclusion These new data have implications for our understanding of the controls on floc dynamics and the function of floc porosity and can improve the parameterisation of current cohesive sediment transport models.

Keywords 3-dimensional · Fractal · Microscopy · Cohesive · Aggregates · Flocculation · Pore network

✉ T. J. Lawrence
   t.lawrence@qmul.ac.uk

1 School of Geography, Queen Mary University of London, Mile End Road, London E1 4NS, UK

2 Institute of Science and Environment, University of Cumbria, Ambleside LA22 9BB, Cumbria, UK

3 HR Wallingford, Howbery Park, Wallingford OX10 8BA, Oxfordshire, UK

4 School of Earth and Environmental Sciences, Cardiff University, Cardiff CF10 3AT, UK

5 River Restoration Centre, Cranfield University, Cranfield MK43 0AL, UK

1 Introduction

Fine cohesive sediment is a globally vital component in the healthy functioning of aquatic systems (Malakoff et al. 2020). It affects a variety of aquatic system features including navigation, aquaculture, aquatic biodiversity, and fisheries (Khangaonkar et al. 2017; De Bruijn 2018; Law and Hill 2019; Gadeken et al. 2021; Zhang et al. 2021). This sediment is largely transported as flocculated suspended sediment or 'flocs', so it is imperative that the characteristics and behaviour of suspended sediment flocs are fully understood.

Flocs are fragile, complex, low-density aggregates of minerogenic and biogenic material with fluid-filled pore space and typically represent the main component of suspended particulate matter (SPM) in systems dominated by fine sediment (Droppo 2001; Burd and Jackson 2009). SPM plays a fundamental role in the fluxes and fate of sediment (Prandle et al. 2005; Manning and Dyer 2007; Spearman et al. 2020), carbon, nutrients (Ussher et al. 2011),

contaminants (Schindler et al. 2021), and pathogens through all natural aquatic environments, and the settling of SPM is the main mechanism for downward flux of carbon in the ocean (Azam and Long 2001). Therefore, understanding floc structure and functional behaviour is essential for the sustainable management of all aquatic environments (Wheatland et al. 2017, 2020; Spencer et al. 2021).

A key component of natural sediment flocs is fluid-filled pore space at micro- and nanometre length scales (Wheatland et al. 2017, 2020; Ho et al. 2022). Porosity both creates drag and influences buoyancy meaning that porosity can have significant influence on floc settling behaviour, floc stability, and compaction once settled (Moruzzi et al. 2020). Therefore, it is critical to understand and quantify these structural floc features. However, there are currently no effective means by which pore space within flocs can be measured, because flocs are fragile making them difficult to sample without damaging their structure, and 3D in nature meaning they are difficult to observe and quantify (Droppo 2004; Amarasinghe et al. 2015). As a result, porosity values tend to be an inferred property estimated from measures of 2D size and settling velocity assuming spherical shape (Hsu and Liu 2010; Fromant et al. 2017). This introduces considerable uncertainty in the validity of sediment transport and contaminant models, as they are compromised by a lack of directly observed data on porosity and pore spaces which they rely on for reliable and accurate outputs (Warner et al. 2008; Ye et al. 2018; Vowinckel et al. 2019; Zhu 2019). Conventionally, bulk porosity (Droppo et al. 2000; Hsu and Liu 2010) and pore diameter (Liss et al. 1996; Williams et al. 2008; Chen et al. 2012) have been measured in flocs, and in clay-rich soils and sediments more broadly (Kozlowski and Ludynia 2019; Obour et al. 2019).

Floc structures can now be stabilised, imaged, and quantified in 3D using µCT techniques (Wheatland et al. 2017, 2020; Zhang et al. 2018; Spencer et al. 2021). The advent of these new imaging techniques allows the exploration and interrogation of both bulk porosity, and pore-space and pore-network characteristics.

The overall aim of this study was to quantify the complex 3D structural characteristics of pore space in natural sediment flocs using volumetric microtomography. Specifically, we quantify porosity, pore space (diameter and shape), and pore network characteristics (tortuosity and connectivity) and define hydraulically effective and isolated pore space associated with flocs. The parameter data in this project were produced using volumetric measurements, where image data was segmented and measured in 3D volume, rather than using 2D inferences or proxies. These novel data provide insights into the hydraulic functioning of floc porosity, could improve parameterisation of current cohesive sediment transport and flocculation models, and improve understanding of floc behaviour.

2 Methods

The overarching theme of the methodology was to image, characterise, and quantify pore properties of natural sediment flocs in 3D and compare these novel data to porosity inferred from settling velocity and 2D floc diameter generated using conventional approaches (Manning et al. 2007, 2011; Ye et al. 2018).
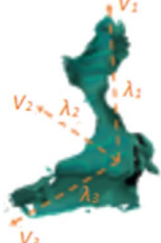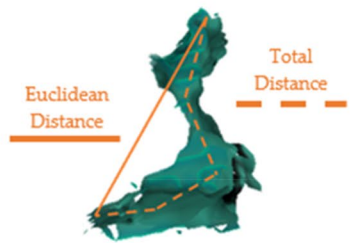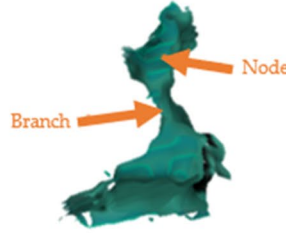
2.1 Experimental setup

The natural sediment flocs used in this study were formed in the lab using an annular flume (Fig. S1a) from fine grained mud-flat sediment collected from the Thames Estuary, SE England. Sediment from this area has been reported as silty clays with LOI values typically < 10% (O'Shea et al. 2018), containing total organic carbon of 1% (Lopes dos Santos and Vane 2016). Prior to carrying out experiments, the sediment was stored at < 4 °C to discourage bacterial activity. When mixing in the flume, artificial seawater (Sigma Sea Salts) was used (salinity 34 g L^{-1}) to recreate estuarine conditions. 2D and 3D datasets were combined by sub-sampling flocs for 3D analysis from 2D-observed populations. 2D datasets included inferred bulk porosity and Feret diameter-based floc size, and 3D datasets included directly measured porosity, volumetric floc size, 3D measured pore diameter, shape, tortuosity, and connectivity (Fig. 1).

2.2 2D data collection

To calculate settling velocity and to retain samples for subsequent post-settling 3D image acquisition, a modified version of the LabSFLOC-2 (Manning 2006; Manning et al. 2007, 2017) high-resolution (1 pixel = 6 mm) video floc camera system was employed (Fig. S2b). Immediately prior to LabSFLOC-2 experimentation, the flocs were re-suspended for 10 min within the annular flume. Flocs were sub-sampled from the flume-based floc population using a broad aperture pipette (Gratiot and Manning 2007), which was subsequently fixed in place above the LabSFLOC-2 column, in contact with ~ 0.5 cm depth of water. The LabSFLOC-2 system records flocs settling past a high-definition camera and video files are stored for later processing (Manning 2006; Ye et al. 2018, 2020), creating the raw 2D detailed video (.AVI format) dataset. To collect a set of floc samples for 3D image assessment, the method outlined by Droppo et al. (1996) was used, whereby a plankton chamber was placed at the base of the LabSFLOC-2 column to collect sediment (Fig. S2b), before the flocs were immobilised in agarose gel.

Fig. 1 3D pore space features that have been measured, and the method by which the data was collected, along with a brief description of how the data was processed into the pore space parameters required

Parameter	Units	Measurement method (BoneJ)	Representation of measurement process in 3D	Process Notes
Porosity (& 3D Floc and Total Pore Volume Size)	μm^3	Volume Fraction		Floc and pore space 3D volumes are quantified. Porosity calculated by: (pore vol/floc vol) *100.
Pore Diameter	μm	Mean Thickness (T_m)	$T_m = t_1 + t_2 + t_3 ... / t_n$	T_m value for each individual pore in output tables. Median of these mean values can also be used to represent the pore spaces within any given individual floc.
Pore Shape	n/a	Principal centroidal axes measurements ($\lambda_1, \lambda_2, \lambda_3$)		Tri-plot (Graham & Midgley, 2000) to represent data. Axes are plotted onto an adapted Ternary diagram, the split of which is: disk, rod & sphere.
Pore Tortuosity	n/a	Euclidean & total distance by analyze skeleton		Tortuosity = total length of pore space/Euclidean distance (measured at the extreme of centroidal vertices).
Pore Connectivity	b/n	Number of branches and nodes by analyse skeleton		Connectivity = no. of pore branches/no. of pore nodes.

2.3 3D data acquisition

An established block staining protocol (Wheatland et al. 2017) was used to prepare floc samples for µCT vacuum condition scanning. The samples collected from the plankton chamber in the LabSFLOC-2 system were immobilised in agarose to prevent structural alteration, and subsequently stained using heavy metals (including uranyl acetate), before dehydration and resin embedding. This process is a well-established approach (Wheatland 2016; Wheatland et al. 2017, 2020; Spencer et al. 2021) that has been demonstrated to preserve floc structure. The staining process enhances contrast between organic and inorganic constituents in µCT scan images (Wheatland et al. 2020).

The resin-embedded samples were scanned using a Nikon Metrology XT-H 225 (NikonMetrology 2020), fitted with a transmission target. The scans were performed at a voltage of 150 kV and a current of 160 µA to optimise contrast and resolution (Wheatland et al. 2020; Spencer et al. 2021, 2022), resulting in a scan resolution of 2.78 µm. The scans were reconstructed using CTPro3D (NikonMetrology 2013) before post-processing and data analyses were performed using ImageJ/Fiji v2.35 (Schindelin et al. 2012), including BoneJ v1 (Doube et al. 2010).

Due to the time constraints of data processing, a floc subsample was selected at random from the agarose block during the stabilisation and staining procedure, and at the µCT image analysis stage, 30 flocs were selected at percentile intervals. The 25th and 75th percentiles of micro-flocs, and the 25th, 50th, and 75th percentiles of macro-flocs, were used. This provided 150 segmented floc samples for analysis.

2.4 Data processing and analysis

The settling video files collected by the LabSFLOC-2 were used to generate 2D floc size (Feret diameter) and settling velocity data for individual flocs through a combination of the Weka Trainable Segmentation (Arganda-Carreras et al. 2017) and TrackMate (Tinevez et al. 2017) plugins within ImageJ (Lawrence 2021). Floc effective density and inferred porosity were then estimated using an adaptation of Stokes' law (Manning et al. 2011; Soulsby et al. 2013). To enable comparison, the 2D floc data were sub-sampled using the same approximate Feret diameter size ranges.

3D quantification of floc porosity consisted of a series of operations performed on the segmented floc volume using the BoneJ (Doube et al. 2010) and MorphoLibJ (Legland et al. 2016) plugins within ImageJ. A summary of the parameters measured in the 3D floc samples is presented in Fig. 1.

Here, bulk porosity % was measured using the floc and pore space volume outputs from the 'volume fraction' measurement tool in BoneJ: (total pore volume/total floc volume) *100. Hydraulically 'effective' and 'isolated' pore volumes were defined and segmented. Pores were deemed to be hydraulically effective if they were connected to the exterior surface of the floc and hence the transporting medium, and isolated pores were defined by being entirely enclosed within the floc structure.

The individual pore spaces of each floc were similarly measured as a part of the total porosity and segmented into hydraulically effective and isolated pore space. Individual pore volumes were extracted from the total pore volume data. Pore diameter is the mean average value summarised from a series of maximum-fit spherical diameter measurements taken along the length of the pore (Dougherty and Kunzelmann 2007; Doube et al. 2010). Pore shape was assessed by adapting the approach commonly used for clast

analysis (Graham and Midgley 2000) whereby objects are plotted in a continuum between spherical, rod, and plate shape end members. Rather than the C_{40} index as applied to clasts to indicate degree of wear, in this study, a B_{60} index is used to determine the proportion of pores that are rod-shaped (Lawrence 2021). This is an important measure as it can indicate elongation of the pores, which could influence hydraulic efficiency.

Pore network properties were generated by conversion of the pores associated with each floc into a topological network through skeletonisation (Arganda-Carreras et al. 2010). This enabled quantification of pore tortuosity and connectivity, thus characterising pore network complexity and efficiency (Fig. 1).

3 Results and discussion

Floc size and porosity data were collected for 963 flocs in 2D, and floc size, porosity, pore space, and pore network data were collected for 150 flocs in 3D.

3.1 Floc porosity

Floc porosity distributions for the floc populations measured in both 2D and 3D are presented in Fig. 2.

The inset images in Fig. 2 depict representations of the methodological approach applied to floc samples to gain the porosity data. In panel a, the inset image shows a Feret diameter-based ellipsoid applied to the floc, to gain inference of floc density as a porosity proxy. In panel b, a 3D rendered image (using Drishti (Limaye 2012)) of directly measured 3D porosity is shown. Figure 2 a shows that 2D-inferred porosity values ranged between 0.4 and 98%, with a mean value of 55% and a median value of 58%. Porosity derived from 3D measurements ranged between 4 and 52%, with mean and median values of 24% (Fig. 2b). These distributions are markedly different. Porosity values inferred using 2D approaches estimated from settling velocity are consistent with those reported in the literature for natural sediment flocs (Syvitski et al. 1995; Droppo et al. 1997; Manning et al. 2004; Spencer et al. 2010), indicative of loosely-bound, highly porous sediment aggregates (Stone et al. 2008). By contrast, porosity values observed and quantified from 3D volumes have substantially lower range, mean and median values indicating that porosity values are lower and less variable in natural sediment flocs than previously considered.

These 3D observations demonstrate that floc porosity values derived from 2D floc settling velocity, systematically and substantially over-estimate floc porosity quantified from 3D floc volumes. There may be two explanations for this. Firstly, porosity is estimated in 2D by fitting an ellipsoid to the floc 2D projection to estimate diameter (panel 'a'
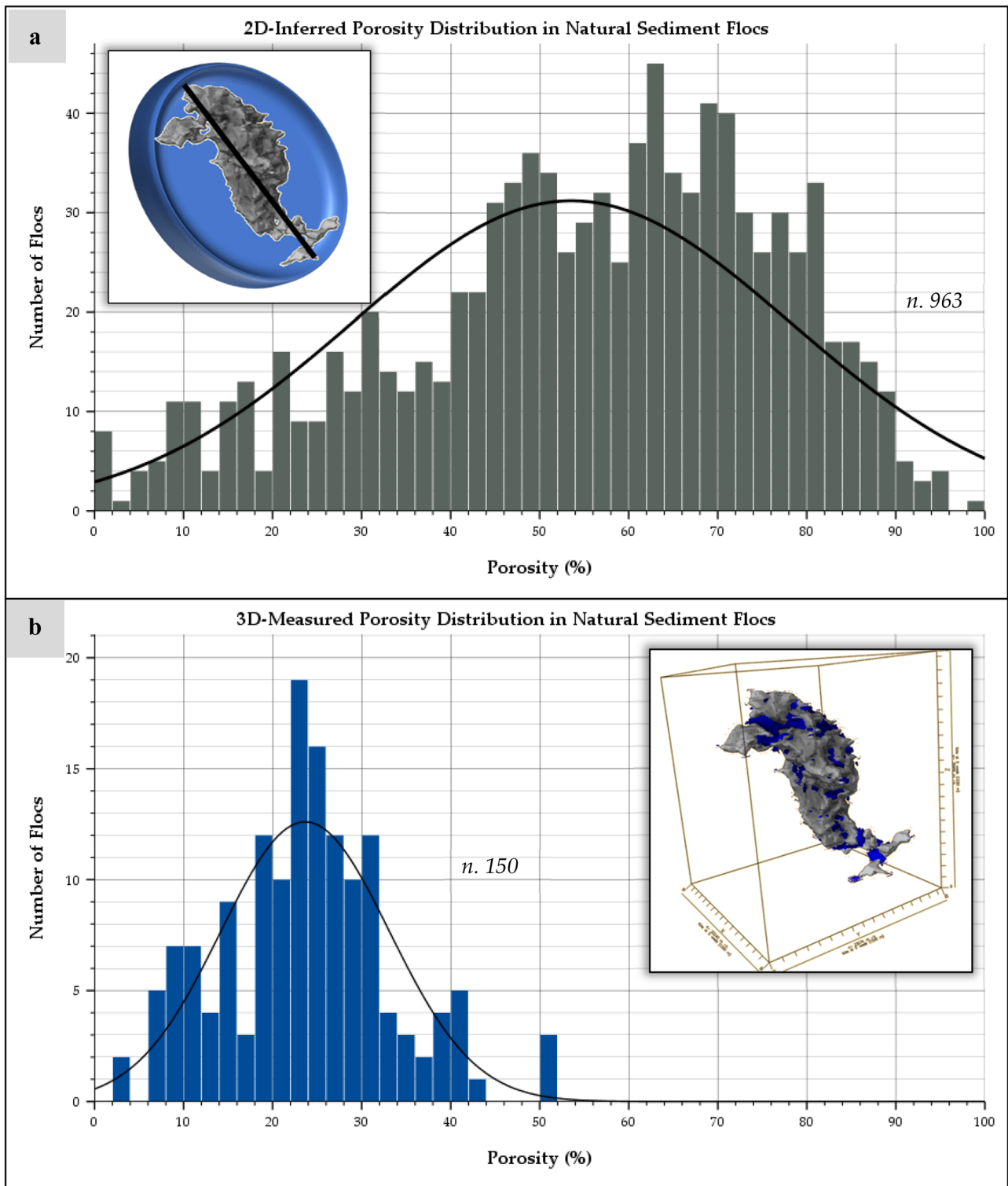
Fig. 2 Porosity (%) distribution measured by indirect 2D (top) and direct 3D (bottom) methods. A normal distribution line has been included in both plots. Inset top panel: representation of conventional 2D method applied to a floc. Inset bottom panel: rendered image of 3D-measurement method applied to the same natural floc

inset, Fig. 2). For simple, near-spherical flocs, this may not be problematic. However, we know from our previous 3D examinations of natural sediment flocs that floc shape is far more irregular and less spherical than previously thought (Wheatland et al. 2017, 2020; Zhang et al. 2018; Spencer et al. 2021) and therefore, fitting an ellipsoid (or sphere) will incorporate significant external space over-estimating floc porosity. This external space has no function in terms of either floc buoyancy or fluid flow through the floc yet is included in 2D inferential porosity calculations. If porosity is over-estimated, then, by default, we must also be under-estimating floc density. Here, porosity is easily segmented from other floc phases as unoccupied space; however, measuring density in the same way becomes much more challenging due to the heterogeneous nature of solid material in the flocs. Secondly, μCT detection limits preclude observation and quantification of nano-porosity which has been estimated at typically < 10% of total floc porosity (Wheatland et al. 2020). However, much of the nano- and micro-scale pore space in flocs is filled with EPS (Wheatland et al. 2020), so not all nano-porosity is viable as 'empty' space. This creates a conceptual point for consideration: 'what constitutes "true" porosity?'. If we are focusing on packing spaces between molecules or nano-scale particles, then how much does this influence buoyancy and hydraulic conductivity?

The lower values of quantified porosity in these sediments are likely to be a combination of these two effects. Therefore, current models which predict floc behaviour (settling velocity, flocculation) may be using over-estimates of porosity and under-estimates of density. These parameters are used as inputs to sediment settling models and help to determine the modelled hydrodynamic behaviour of flocs including settling velocity, susceptibility to drag and shear forces, and torsional force effects on the floc structure. This limits the power with which the models can predict sediment settling patterns and implies that other structural characteristics such as floc shape may be more important. This project dealt with one population of flocs, and flocs with different composition and different environmental conditions may display very different pore characteristics and/or functional behaviours.

An important factor in the consideration of floc behaviour is the relationship between floc size and porosity, with floc density decreasing and porosity increasing with floc size as pore space is incorporated with floc growth resulting in large, fragile, 'loose' flocs structures (Winterwerp 1998; Khelifa and Hill 2006; Jin et al. 2012; Vahedi and Gorczyca 2012; Zhu et al. 2018). Flocs are considered to have fractal geometry and fractal-based models which assume structural self-similarity across multiple scales are widely used to predict floc behaviour (e.g. settling velocity, rate of floc aggregation and disaggregation) (Perfect and Kay 1995).

The relationship between porosity and floc size is shown in Fig. 3a (porosity and size generated from 2D data) which shows a strong, positive relationship between porosity and floc size (Gorczyca 2000; Liao et al. 2000). Porosity increases with floc diameter and the largest porosity values are represented in the largest macro-flocs, a relationship reported in the literature (Droppo et al. 2000; Gorczyca 2000; Cui et al. 2019; Filipenska et al. 2019; Moruzzi et al. 2020). The two groups of data (Fig. 3a) are an artefact of the sampling method used, with flocs sampled from micro- and macro-floc size intervals (Sect. 3.3). In contrast, when examining the 3D data (Fig. 3b), the relationship between floc size and porosity is weaker, with considerable data variability, illustrated by the expanding cone shape seen in the dashed lines that mark the 'edges' of the data spread. This again is likely to be due to the use of the Feret diameter to estimate floc size and hence incorporate external empty space into the floc volume. The two groups of data represent the micro-(grey)/macro-(gold) floc split from the sampling strategy.

For small, compact, near-spherical micro-flocs (Spencer et al. 2021), the Feret diameter-based ellipsoid method is likely to provide a better estimation of floc size, but as flocs get larger and more complex, over-estimation of porosity is likely to increase as more external empty space is included in the calculation. This will be most apparent for large, organic-rich natural flocs with highly irregular shapes. Therefore, well-documented observations of positive relationships between floc size and porosity may be largely due to the use of 2D ellipsoid fitting of increasingly irregularly shaped flocs.

3.2 Individual 3D pore morphology

One of the additional benefits of the direct imaging of individual flocs in 3D is the interrogation of the morphological characteristics of individual pores. This object-based analysis holds advantage over sampling analysis as subtleties of finer-scale features are quantifiable, and such features can exert significant influence over gross-scale functionality and behaviour (Taylor et al. 2017).

Most (68%) pores measured between 5.4 and 5.6 μm wide, with an overall range of 5.4–12.6 μm (Fig. S2). Individual pore volumes were predominantly within the 0–5000 μm^3 range, with a long data tail to the maximum value c. 330,000 μm^3. Most of the tail of data consists of small peaks of 1–5 pores, indicating a higher degree of variability beyond the initial dominant peak. Pore shape analysis (ratio of a, b, and c axis, see Fig. S4) showed that 61.7% of pores were rod-shaped, i.e. elongated, with the remainder spread variably throughout the other shape categories (sphere and disc).
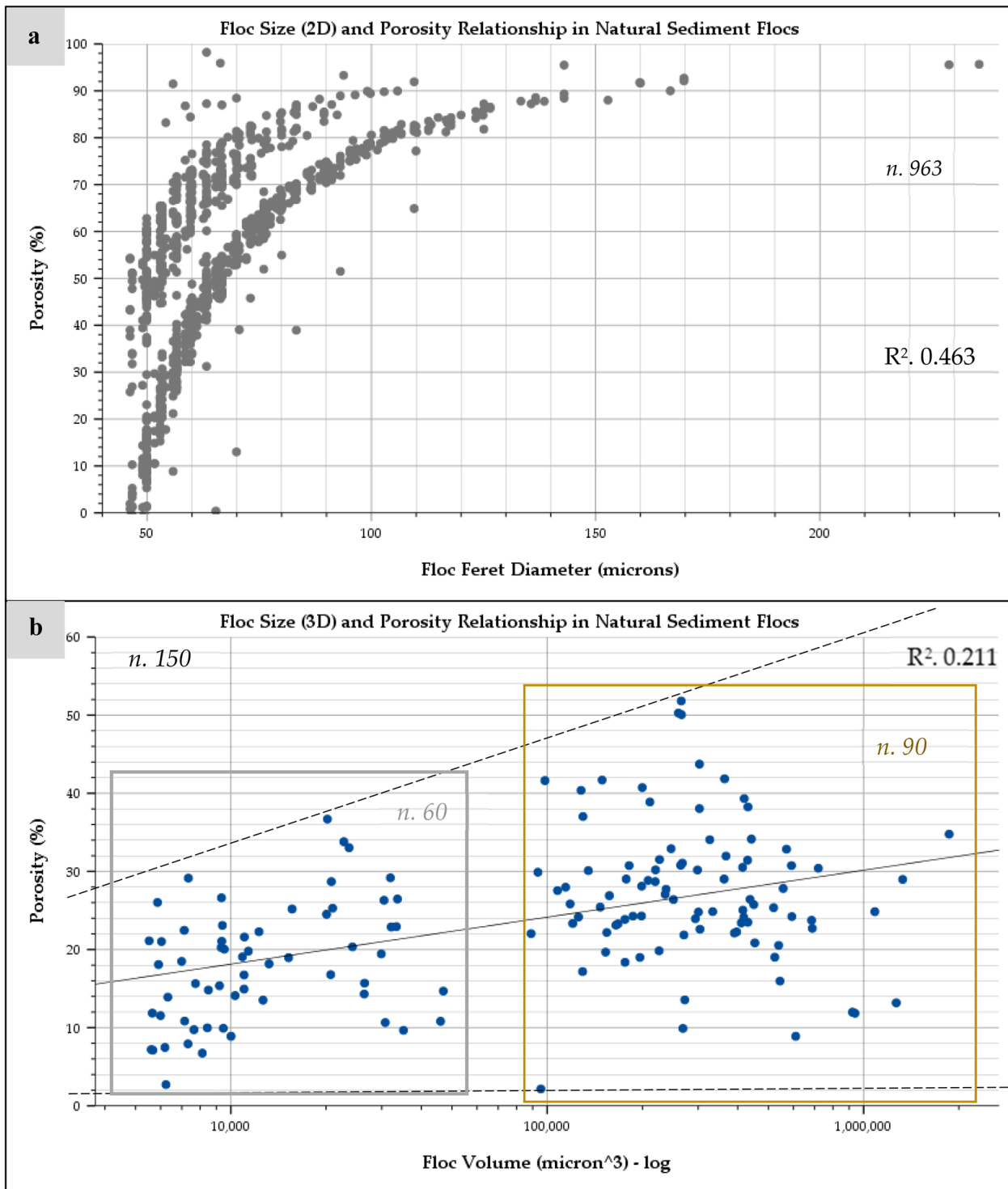
Fig. 3 Floc size and porosity relationship measured by 2D methods (top panel) and 3D methods (bottom panel). Floc Feret diameter and effective density-inferred porosity are plotted in the top panel, and 3D directly quantified floc volume and porosity are plotted in the bottom panel. The grey (micro-flocs) and gold (macro-flocs) boxes indicate the divide in the sampling strategy

These datasets tie together to form a multivariate description of, and explanation for, individual pore morphology. Pores are created by the initial aggregation process of flocs and deposition and resuspension cycles that the sediment subsequently experiences (Mooneyham and Strom 2018). They are important hydrodynamically for their contribution

to floc settling behaviour (Gregory 1997; Droppo et al. 2008), as their size not only determines hydrodynamic efficiency of advective flow through the floc, but floc density and stability are also affected by pore size (Wu et al. 2006; Taamneh and Bataineh 2011; Zhang and Zhang 2015). Pores also facilitate the transport and exchange of pollutants, contaminants and gases (Droppo and Leppard 2004; Koji 2012; Wang et al. 2020), so their size and shape are important factors in floc structure and behaviour. Flocs with predominantly rod-shaped pores are likely to comprise of many loosely bound, elongated structures such as EPS and bacterial linkages between smaller nodes of sediment, whereas flocs with highly variable pore shapes, with less-rod-shaped pores are more likely to be simpler, possible denser flocs with pores positioned predominantly within sediment clusters. Here, pore diameter ranges from 5 to 12.6 μm, but the volume data spreads over three orders of magnitude, and this is explained by the dominance of rod-shaped pores with otherwise substantial shape variability. Rod-shaped pores bear a similar diameter regardless of their length, with the length causing the variation in pore volume. These predominantly elongated micro-scale pores are indicative of a floc structure that is 'looser', more complex, more heterogeneous, and influenced by flocculation mechanisms beyond the electrochemical flocculation that is typical of smaller flocs with more compact pore spaces (Spencer et al. 2021).

3.3 3D pore network characteristics

Beyond bulk porosity % and individual pore space morphology, pore network characteristics are an important aspect of floc porosity. Pore tortuosity and connectivity can offer insights into the network characteristics of pore spaces within the floc structure (Meyers et al. 2001). Pore tortuosity can determine the rate at which advective flow is possible through floc structures, and this affects both settling velocity and floc stability (Yang et al. 2006; Appelo et al. 2010). Connectivity in this context is an indicator of pore network complexity and is a useful indicator of overall permeability of a sediment structure which as implications for stability and erodibility (Liu et al. 2013), in addition to contributing to the hydraulic conductivity of a floc during settling (Dai and Santamarina 2013; Lozano et al. 2013; Li et al. 2019; Lu et al. 2019; Lucas et al. 2020).

Most pores have low tortuosity (Fig. S3a), with ~ 75% of the pores displaying a tortuosity value between 1 and 1.5, with c. 25% of pores having higher tortuosity up to 6.8. Figure S3b indicates that almost a third of pores are very well-connected (few dead-ends or low complexity), with a value of 1. The smaller peak at 2, surrounded by a leptokurtic distribution of other data values, accounts for much of the remainder of the data. Rare instances of poor connectivity are present however, with 5% of the pores registering connectivity values of 3–4.

Water flow through any porous media, e.g. soils, is dependent upon the pore diameter and distribution (friction) and the length and tortuosity of flow pathways (Childs and Collis-George 1950; Shein 2010). Here, the pore network data assesses the degree to which water can flow through floc pores and hence influences drag and settling rates of suspended material (Strom and Keyvani 2011), and possibly the exchange of nutrients, waste products, and contaminants to bacteria within the floc. Here, low tortuosity values indicate that most pores will provide little resistance, meaning advective flow through the floc is achieved with little interference, and as such, the drag experienced by the floc as a whole is reduced (Burger et al. 2017; Zhao et al. 2018). Very high tortuosity can turn an otherwise hydraulically viable pore system into a hydraulically resistant or 'closed' system, due to water being slowed to an extent that it would not flow within the timescale of a floc settling event. This causes other parameters of that system such as pore diameter to become irrelevant. Figure S3b shows that c. 30% of the pores have very low connectivity indicating that water could move through a simple pathway. Again however, there are examples of very complex pore networks with a high potential for dead-end passageways that would impede hydraulic flow. These datasets can be used in conjunction with other parameters to inform the internal hydraulic potential of a floc but can also be important individually. The pore network parameters can provide a direct input to sediment settling models as they are values that can determine the ease at which water can move through the floc structure. This is a completely new insight that would be unavailable using only gross-porosity (%) measures of pore space.

3.4 Pore typology: distinguishing between hydraulically effective and isolated pore space

The morphological and network properties outlined above introduce the idea that porosity may have a structural impact on the passage of water through a floc falling through the water column. These factors enact this influence by retarding settling as a function of increasing buoyancy or enhancing settling by efficiently allowing transit of water through the overall floc space (Droppo et al. 2000; Chu et al. 2005; Moruzzi et al. 2020). To assess whether pore space is contributing buoyancy to the settling floc requires establishment of whether a pore is hydraulically effective or isolated from the exterior of the floc. Pores were classified as effective (connection to the floc exterior hence allowing fluid exchange with the surrounding transport media), or isolated. Ninety-nine percent of the total pore volume was hydraulically effective pore space.

The effective porosity is normally distributed (Fig. 4a), ranging from 2 to 52% with a modal peak at 24%. Isolated porosity is < 3% of the total porosity. This difference is statistically significant for both median value (Independent Standard Median test sig. 0.000) and range (Kruskal–Wallis sig. 0.000) tests. Therefore, most pores in natural sediment flocs are hydraulically connected to the transporting medium potentially allowing water to flow through the floc.
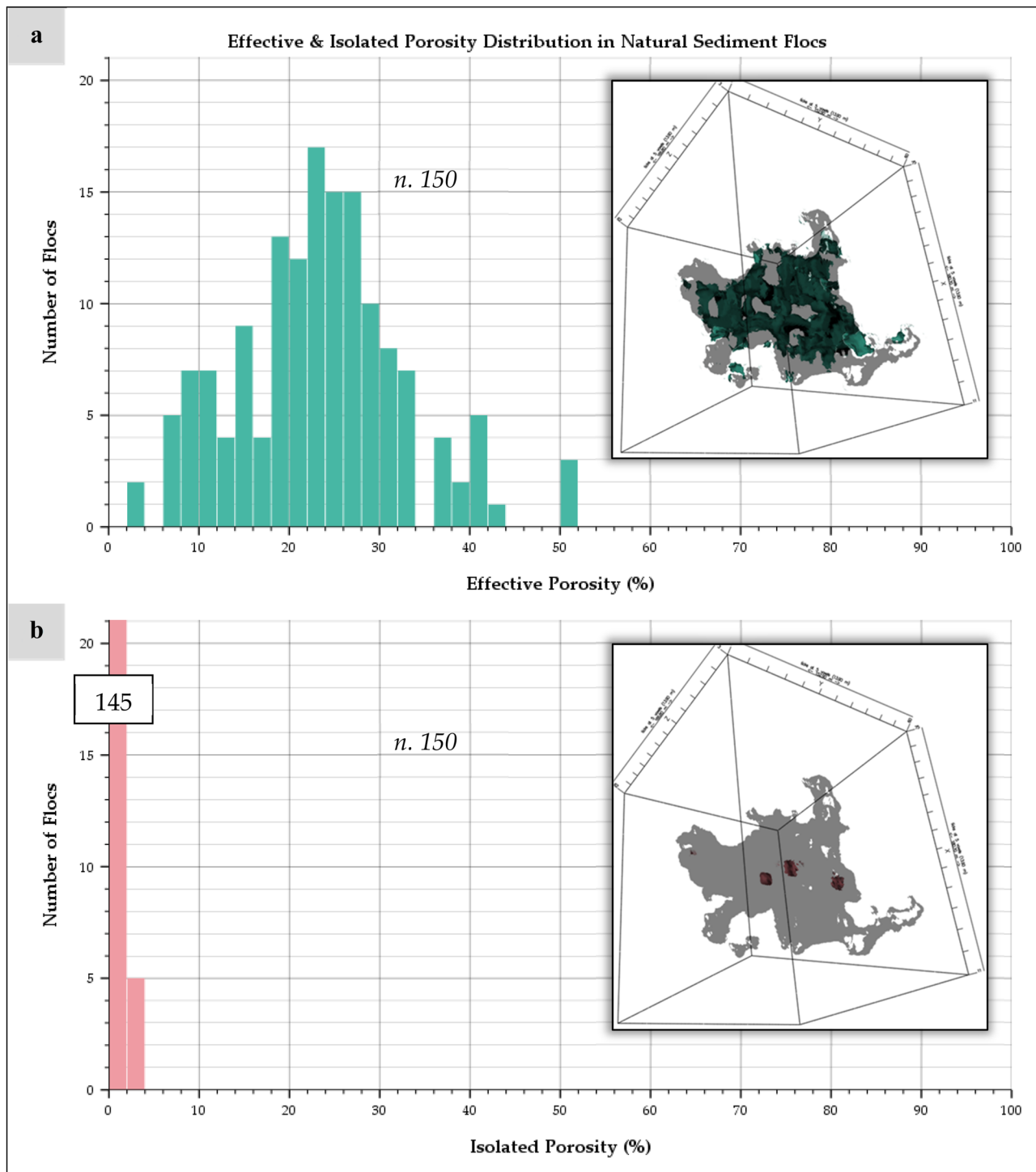
Fig. 4 Effective (green) and isolated (pink) pore volume % proportion distribution in natural sediment flocs. Inset: 3D renderings of effective and isolated pore volume from the same natural sediment floc (grey) volume. The "145" annotation on the isolated porosity plot indicates the number of data points that fall within the lowest bin category of 0–2% porosity

The morphological and network characteristics of these effective pores are likely to influence the efficiency of water flow through the floc, and thus influence settling velocity and therefore functional behaviour.

Typically, effective pores occupy a higher percentage of the floc structure with mean porosity value of 25.3% vs 0.4% for isolated pores; are wider with a mean diameter of 7.28 µm vs 5.2 µm for isolated pores; and are less well-connected with a mean connectivity value of 1.78 compared to 1.31 in isolated pores. There is little difference between the two pore types. Additionally, almost all hydraulically isolated pore spaces possess a volume < 10,000 µm^3, but only around half of effective pore spaces sit within this size range. The effective pore space volumes are distributed over a larger range, up to 340,000 µm^3, but isolated pore space volume maxima sit within the 10,000–20,000 µm^3 range.

Both effective and isolated pore space shape indices are dominated by rod-shaped pores (Fig. 5), but effective pore spaces tend to be more rod-shaped than isolated pore spaces. The distributions also show that extreme shape values, such as those that are plotted in the disk and sphere corners of the plot, are isolated pore spaces.

The two pore typologies display very different characteristics, and the prevalence of effective pore spaces indicates that most natural floc pores can contribute to fluid, contaminant, pollutant, and nutrient transport. The position of these effective pores at the periphery of floc structures, combined with their larger size, has implications for density distribution in the floc, and as such, floc behaviour (Gregory 1997; Droppo 2004; Droppo et al. 2008; Burger et al. 2017). An area for further investigation, which would provide better input for floc settling behaviour modelling, is to determine the proportion of the effective pore spaces that are connected

to the outside of the floc in a minimum of two locations. The typology of pores within flocs and the bulk, morphological, and network properties of such pore space identified in this study enable us to consider how pore spaces influence functional behaviour, particularly the settling rate of flocs. Consequently, the application of the porosity properties examined here can be applied to understand the differences in observed settling experiments and for different compositions and sizes/shapes of flocs.

To conclude, novel µCT approaches have enabled the quantification of porosity, pore space, and pore network characteristics of natural sediment flocs. These new data demonstrate that conventional estimates of porosity derived from observations of 2D floc size and settling velocity over-estimate the porosity of natural suspended sediment flocs by around 30% and have a weaker relationship with floc size than previously thought. This is most likely due to the use of ellipsoid fitting to measure floc size resulting in an under-estimation of floc shape complexity which is most significant for large, complex macro-flocs. This implies that floc density is also being under-estimated. This has implications for our understanding of the role of porosity in floc dynamics and the accuracy of porosity data (and potentially density) currently being used in mathematical models that predict cohesive sediment dynamics. Most pore space was hydraulically effective enabling flow through the internal floc structure and contributing to fluid, contaminant, and nutrient transport. This also highlights the importance of modelling flocs as porous media rather than solid particles and considering the influence of drag on settling velocity. This study has also provided unprecedented characterisation of pore size, shape, and variability and offers the potential for future investigations of the influence of these parameters

Fig. 5 Pore space shape distribution in natural flocs, divided into hydraulically effective and isolated pore spaces. Circle in effective pore shape plot indicates a zone where a large portion of the n is situated
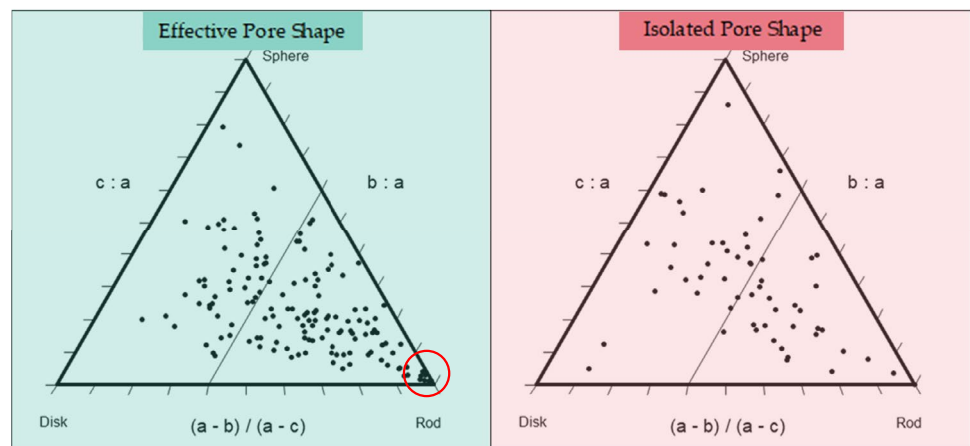
Pore Shape (B60 index)	Total Pores	Effective Pores	Isolated Pores
Natural Flocs	61.7%	66.2%	50.0%
Pores n	206	148	58

on floc stability, settling behaviour, and compaction and how this might vary with floc composition. Finally, these new data enable us to question how we define porosity in flocs and what we classify as void space.

Declarations

Competing interests The authors declare no competing interests.

References

Amarasinghe PM, Abelev A, Qadri SB, Calantoni J (2015) Micromechanical determination of the tensile strength of flocculated artificial marine cohesive sediment. Mech Res Commun 64:42–49. https://doi.org/10.1016/j.mechrescom.2015.01.002

Appelo CAJ, Van Loon LR, Wersin P (2010) Multicomponent diffusion of a suite of tracers (HTO, Cl, Br, I, Na, Sr, Cs) in a single sample of Opalinus Clay. Geochim Cosmochim Acta 74:1201–1219. https://doi.org/10.1016/j.gca.2009.11.013

Arganda-Carreras I, Fernández-González R, Muñoz-Barrutia A, Ortiz-De-Solorzano C (2010) 3D reconstruction of histological sections: application to mammary gland tissue. Microsc Res Tech 73:1019–1029. https://doi.org/10.1002/jemt.20829

Arganda-Carreras I, Kaynig V, Rueden C et al (2017) Trainable Weka Segmentation: a machine learning tool for microscopy pixel classification. Bioinformatics 33:2424–2426. https://doi.org/10.1093/bioinformatics/btx180

Azam F, Long RA (2001) Oceanography: sea snow microcosms. Nature 414:495–498

Burd AB, Jackson GA (2009) Particle Aggregation Ann Rev Mar Sci 1:65–90. https://doi.org/10.1146/annurev.marine.010908.163904

Burger W, Krysiak-Baltyn K, Scales PJ et al (2017) The influence of protruding filamentous bacteria on floc stability and solid-liquid separation in the activated sludge process. Water Res 123:578–585. https://doi.org/10.1016/j.watres.2017.06.063

Chen M, Yang G, Chai Z (2012) Study on pore characteristic of silt floc based on SEM image. World Autom Congr Proc 2012:1–4

Childs EC, Collis-George N (1950) The permeability of porous materials. Proc R Soc London Ser A Math Phys Sci 201:392–405. https://doi.org/10.1098/rspa.1950.0068

Chu CP, Lee DJ, Tay JH (2005) Floc model and intrafloc flow. Chem Eng Sci 60:565–575. https://doi.org/10.1016/j.ces.2004.07.132

Cui Y, Ravnik J, Steinmann P, Hriberšek M (2019) Settling characteristics of nonspherical porous sludge flocs with nonhomogeneous mass distribution. Water Res 158:159–170. https://doi.org/10.1016/j.watres.2019.04.017

Dai S, Santamarina JC (2013) Water retention curve for hydrate-bearing sediments. Geophys Res Lett 40:5637–5641. https://doi.org/10.1002/2013GL057884

De Bruijn L (2018) Maintenance dredging in the Port of Rotterdam: a research into the increase in maintenance dredging volume at the Port of Rotterdam. PhD Thesis, Delft University of Technology

Doube M, Klosowski MM, Arganda-Carreras I et al (2010) BoneJ: Free and extensible bone image analysis in ImageJ. Bone 47:1076–1079. https://doi.org/10.1016/j.bone.2010.08.023

Dougherty R, Kunzelmann K-H (2007) Computing local thickness of 3D structures with ImageJ. Microsc Microanal 13:1678–1679. https://doi.org/10.1017/s1431927607074430

Droppo IG (2001) Rethinking what constitutes suspended sediment. Hydrol Process 15:1551–1564. https://doi.org/10.1002/hyp.228

Droppo IG (2004) Structural controls on floc strength and transport. Can J Civ Eng 31:569–578. https://doi.org/10.1139/L04-015

Droppo IG, Exall K, Stafford K (2008) Effects of chemical amendments on aquatic floc structure, settling and strength. Water Res 42:169–179. https://doi.org/10.1016/j.watres.2007.06.054

Droppo IG, Flannigan DT, Leppard GG et al (1996) Floc stabilization for multiple microscopic techniques. Appl Environ Microbiol 62:3508–3515. https://doi.org/10.1128/aem.62.9.3508-3515.1996

Droppo IG, Leppard GG (2004) Sediment-contaminant interactions and transport: a new perspective. IAHS-AISH Publ 288:429–436

Droppo IG, Leppard GG, Flannigan DT, Liss SN (1997) The freshwater floc: a functional relationship of water and organic and inorganic floc constituents affecting suspended sediment properties. Water, Air, Soil Pollut 99:43–53. https://doi.org/10.1007/bf02406843

Droppo IG, Walling DE, Ongley ED (2000) The influence of floc size, density and porosity on sediment and contaminant transport. IAHS-AISH Publ 263:141–147

Filipenska M, Vasatova P, Pivokonska L et al (2019) Influence of COM-peptides/proteins on the properties of flocs formed at different shear rates. J Environ Sci (china) 80:116–127. https://doi.org/10.1016/j.jes.2018.11.025

Fromant G, Floc'h F, Lebourges-Dhaussy A et al (2017) In situ quantification of the suspended load of estuarine aggregates from multi-frequency acoustic inversions. J Atmos Ocean Technol 34:1625–1643. https://doi.org/10.1175/JTECH-D-16-0079.1

Gadeken K, Dykstra S, Hagemeyer A et al (2021) Transport of biodeposits and bethic footprint around an oyster farm, Damariscotta Estuary. Maine Peerj 9:e11862. https://doi.org/10.7717/peerj.11862

Gorczyca B (2000) Porosity and structure of alum coagulation and activated sludge flocs. Natl Libr Canada 5–15

Graham DJ, Midgley NG (2000) Graphical representation of particle shape using triangular diagrams: an excel spreadsheet method. Earth Surf Process Landforms 25:1473–1477. https://doi.org/10.

1002/1096-9837(200012)25:13%3c1473::AID-ESP158%3e3.0. CO;2-C

Gratiot N, Manning AJ (2007) A laboratory study of dilute suspension mud floc characteristics in an oscillatory diffusive turbulent flow. J Coast Res 1142–1146

Gregory J (1997) The density of particle aggregates. Water Sci Technol 36:1–13. https://doi.org/10.1016/S0273-1223(97)00452-6

Ho QN, Fettweis M, Spencer KL, Lee BJ (2022) Flocculation with heterogeneous composition in water environments: a review. Water Res 213:118147. https://doi.org/10.1016/j.watres.2022.118147

Hsu RT, Liu JT (2010) In-situ estimations of the density and porosity of flocs of varying sizes in a submarine canyon. Mar Geol 276:105–109. https://doi.org/10.1016/j.margeo.2010.07.003

Jin PK, Zhang K, Wang XC (2012) Fractal characteristics of Al-humic flocs. Desalin Water Treat 42:309–316. https://doi.org/10.5004/dwt.2012.3022

Khangaonkar T, Nugraha A, Hinton S et al (2017) Sediment transport into the Swinomish Navigation Channel, Puget Sound-habitat restoration versus navigation maintenance needs. J Mar Sci Eng 5:19. https://doi.org/10.3390/jmse5020019

Khelifa A, Hill PS (2006) Models for effective density and settling velocity of flocs. J Hydraul Res 44:390–401. https://doi.org/10.1080/00221686.2006.9521690

Koji S (2012) Pollutant and sediment transport caused by turbulent diffusion in rivers and estuaries. Adv Mater Res 374–377:1750–1757. https://doi.org/10.4028/www.scientific.net/AMR.374-377.1750

Kozlowski T, Ludynia A (2019) Permeability coefficient of low permeable soils as a single-variable function of soil parameter. Water (switzerland) 11:2500. https://doi.org/10.3390/w11122500

Law BA, Hill PS (2019) Spatial and temporal variation in cumulative mass eroded and organic matter percentage in surface sediments near areas of active salmon aquaculture. Aquac Environ Interact 11:305–320. https://doi.org/10.3354/aei00315

Lawrence TJ (2021) Quantification of micro-scale floc porosity characteristics utilising 3D microtomography. University of London, Queen Mary

Legland D, Arganda-Carreras I, Andrey P (2016) MorphoLibJ: Integrated library and plugins for mathematical morphology with ImageJ. Bioinformatics 32:3532–3534. https://doi.org/10.1093/bioinformatics/btw413

Li GY, Dai S, Zhan LT, Chen YM (2019) A pore-scale numerical investigation of the effect of pore characteristics on flow properties in soils. J Zhejiang Univ Sci A 20:961–978. https://doi.org/10.1631/jzus.A1900255

Liao BQ, Allen DG, Droppo IG et al (2000) Bound water content of activated sludge and its relationship to solids retention time, floc structure, and surface properties. Water Environ Res 72:722–730. https://doi.org/10.2175/106143000x138346

Limaye A (2012) Drishti: a volume exploration and presentation tool. Dev X-Ray Tomogr VIII 8506:85060X. https://doi.org/10.1117/12.935640

Liss SN, Droppo IG, Flannigan DT, Leppard GG (1996) Floc architecture in wastewater and natural riverine systems. Environ Sci Technol 30:680–686. https://doi.org/10.1021/es950426r

Liu W, Zhao J, Luo Y et al (2013) Experimental measurements of mechanical properties of carbon dioxide hydrate-bearing sediments. Mar Pet Geol 46:201–209. https://doi.org/10.1016/j.marpetgeo.2013.06.016

Lopes dos Santos RA, Vane CH (2016) Signatures of tetraether lipids reveal anthropogenic overprinting of natural organic matter in sediments of the Thames Estuary, UK. Org Geochem 93:68–76. https://doi.org/10.1016/j.orggeochem.2016.01.003

Lozano LA, Soracco CG, Cornelis WM et al (2013) Anisotropy of pore size classes' connectivity related to soil structure under

no tillage. Soil Sci 178:612–617. https://doi.org/10.1097/SS.0000000000000027

Lu J, Wang TH, Cheng WC et al (2019) Permeability anisotropy of loess under influence of dry density and freeze-thaw cycles. Int J Geomech 19:04019103. https://doi.org/10.1061/(ASCE)GM.1943-5622.0001485

Lucas M, Vetterlein D, Vogel HJ, Schlüter S (2020) Revealing pore connectivity across scales and resolutions with X-ray CT. Eur J Soil Sci. https://doi.org/10.1111/ejss.12961

Malakoff D, Desai N, Liu X (2020) Five charts that will change everything you know about mud. Science. https://doi.org/10.1126/science.abe4255

Manning AJ (2006) LabSFLOC - A laboratory system to determine the spectral characteristics of flocculating cohesive sediments. HR Wallingford Technical Report (TR 156).

Manning AJ, Baugh JV, Spearman JR et al (2011) The settling dynamics of flocculating mud-sand mixtures: part 1-Empirical algorithm development. Ocean Dyn 61:311–350. https://doi.org/10.1007/s10236-011-0394-7

Manning AJ, Dyer KR (2007) Mass settling flux of fine sediments in Northern European estuaries: measurements and predictions. Mar Geol 245:107–122. https://doi.org/10.1016/j.margeo.2007.07.005

Manning AJ, Dyer KR, Lafite R, Mikes D (2004) Flocculation measured by video based instruments in the Gironde Estuary during the European Commission SWAMIEE project. J Coast Res 58–69

Manning AJ, Friend PL, Prowse N, Amos CL (2007) Estuarine mud flocculation properties determined using an annular mini-flume and the LabSFLOC system. Cont Shelf Res 27:1080–1095. https://doi.org/10.1016/j.csr.2006.04.011

Manning AJ, Whitehouse RJS, Uncles RJ (2017) Suspended particulate matter: the measurement of flocs. Estuar Coast Hydrogr Sediment Transp 211–260. https://doi.org/10.1017/9781139644426.009

Meyers JJ, Nahar S, Ludlow DK, Liapis AI (2001) Determination of the pore connectivity and pore size distribution and pore spatial distribution of porous chromatographic particles from nitrogen sorption measurements and pore network modelling theory. J Chromatogr A 907:57–71. https://doi.org/10.1016/S0021-9673(00)01018-9

Mooneyham C, Strom K (2018) Deposition of suspended clay to open and sand-filled framework gravel beds in a laboratory flume. Water Resour Res 54:323–344. https://doi.org/10.1002/2017WR020748

Moruzzi RB, Bridgeman J, Silva PAG (2020) A combined experimental and numerical approach to the assessment of floc settling velocity using fractal geometry. Water Sci Technol 81:915–924. https://doi.org/10.2166/wst.2020.171

NikonMetrology (2020) XT H 225 for all-purpose X-ray and CT inspection. https://www.nikonmetrology.com/en-gb/product/xt-h-225

NikonMetrology (2013) CT Pro 3D user manual. Leuven: Nikon

O'Shea FT, Cundy AB, Spencer KL (2018) The contaminant legacy from historic coastal landfills and their potential as sources of diffuse pollution. Mar Pollut Bull 128:446–455. https://doi.org/10.1016/j.marpolbul.2017.12.047

Obour PB, Danso EO, Yakubu A et al (2019) Water retention, air exchange and pore structure characteristics after three years of rice straw biochar application to an acrisol. Soil Sci Soc Am J 83:1664–1671. https://doi.org/10.2136/sssaj2019.07.0230

Perfect E, Kay BD (1995) Applications of fractals in soil and tillage research: a review. Soil Tillage Res 36:1–20. https://doi.org/10.1016/0167-1987(96)81397-3

Prandle D, Lane A, Manning AJ (2005) Estuaries are not so unique. Geophys Res Lett 32:1–5. https://doi.org/10.1029/2005GL024797

Schindelin J, Arganda-Carreras I, Frise E et al (2012) Fiji: An open-source platform for biological-image analysis. Nat Methods 9:676–682. https://doi.org/10.1038/nmeth.2019

Schindler RJ, Comber SDW, Manning AJ (2021) Metal pollutant pathways in cohesive coastal catchments: influence of flocculation and biopolymers on partitioning and flux. Sci Total Environ 795. https://doi.org/10.1016/j.scitotenv.2021.148800

Shein EV (2010) Soil hydrology: Stages of development, current state, and nearest prospects. Eurasian Soil Sci 43:158–167. https://doi.org/10.1134/S1064229310020055

Soulsby RL, Manning AJ, Spearman J, Whitehouse RJS (2013) Settling velocity and mass settling flux of flocculated estuarine sediments. Mar Geol 339:1–12. https://doi.org/10.1016/j.margeo.2013.04.006

Spearman J, Taylor J, Crossouard N et al (2020) Measurement and modelling of deep sea sediment plumes and implications for deep sea mining. Sci Rep 10:5075. https://doi.org/10.1038/s41598-020-61837-y

Spencer KL, Manning AJ, Droppo IG et al (2010) Dynamic interactions between cohesive sediment tracers and natural mud. J Soils Sediments 10:1401–1414. https://doi.org/10.1007/s11368-010-0291-6

Spencer KL, Wheatland JA, Carr SJ, Manning AJ, Bushby AJ, Gu C, Botto L, Lawrence T (2022) Quantification of 3-dimensional structure and properties of flocculated natural suspended sediment. Water Res 118835. https://doi.org/10.1016/j.watres.2022.118835

Spencer KL, Wheatland JAT, Bushby AJ et al (2021) A structure – function based approach to floc hierarchy and evidence for the non - fractal nature of natural sediment flocs. Sci Rep 11:14012. https://doi.org/10.1038/s41598-021-93302-9

Stone M, Krishnappan BG, Emelko MB (2008) The effect of bed age and shear stress on the particle morphology of eroded cohesive river sediment in an annular flume. Water Res 42:4179–4187. https://doi.org/10.1016/j.watres.2008.06.019

Strom K, Keyvani A (2011) An explicit full-range settling velocity equation for mud flocs. J Sediment Res 81:921–934. https://doi.org/10.2110/jsr.2011.62

Syvitski JPM, Asprey KW, Leblanc KWG (1995) In-situ characteristics of particles settling within a deep-water estuary. Deep Res Part II 42:223–256. https://doi.org/10.1016/0967-0645(95)00013-G

Taamneh Y, Bataineh KM (2011) Drag and separation flow past solid sphere with porous shell at moderate Reynolds number. Transp Porous Media 90:869–881. https://doi.org/10.1007/s11242-011-9820-z

Taylor HF, O'Sullivan C, Sim WW, Carr SJ (2017) Sub-particle-scale investigation of seepage in sands. Soils Found 57:439–452

Tinevez JY, Perry N, Schindelin J et al (2017) TrackMate: An open and extensible platform for single-particle tracking. Methods 115:80–90. https://doi.org/10.1016/j.ymeth.2016.09.016

Ussher SJ, Manning AJ, Tappin AD, Fitzsimons MF (2011) Observed dissolved and particulate nitrogen concentrations in a mini flume. Hydrobiologia 672:69–77. https://doi.org/10.1007/s10750-011-0759-4

Vahedi A, Gorczyca B (2012) Predicting the settling velocity of flocs formed in water treatment using multiple fractal dimensions. Water Res 46:4188–4194. https://doi.org/10.1016/j.watres.2012.04.031

Vowinckel B, Withers J, Luzzatto-Fegiz P, Meiburg E (2019) Settling of cohesive sediment: particle-resolved simulations. J Fluid Mech 858:5–44. https://doi.org/10.1017/jfm.2018.757

Wang N, Wang YP, Duan X et al (2020) Controlling factors for the distribution of typical organic pollutants in the surface sediment of a macrotidal bay. Environ Sci Pollut Res 27:28276–28287. https://doi.org/10.1007/s11356-020-09199-w

Warner JC, Sherwood CR, Signell RP et al (2008) Development of a three-dimensional, regional, coupled wave, current, and sediment-transport model. Comput Geosci 34:1284–1306. https://doi.org/10.1016/j.cageo.2008.02.012

Wheatland JAT (2016) Characterising the multi-scale properties of flocculated sediment by x-ray and focused ion beam nano-tomography. PhD Thesis, University of London, Queen Mary

Wheatland JAT, Bushby AJ, Spencer KL (2017) Quantifying the structure and composition of flocculated suspended particulate matter using focused ion beam nanotomography. Environ Sci Technol 51:8917–8925. https://doi.org/10.1021/acs.est.7b00770

Wheatland JAT, Spencer KL, Droppo IG et al (2020) Development of novel 2D and 3D correlative microscopy to characterise the composition and multiscale structure of suspended sediment aggregates. Cont Shelf Res 200:104112. https://doi.org/10.1016/j.csr.2020.104112

Williams ND, Walling DE, Leeks GJL (2008) An analysis of the factors contributing to the settling potential of fine fluvial sediment. Hydrol Process 22:4153–4162. https://doi.org/10.1002/hyp.7015

Winterwerp JC (1998) A simple model for turbulence induced flocculation of cohesive sediment. J Hydraul Res 36:309–326. https://doi.org/10.1080/00221689809498621

Wu RM, Lin MH, Lin HY, Hsu RY (2006) 3D simulations of hydrodynamic drag forces on two porous spheres moving along their centerline. J Colloid Interface Sci 301:227–235. https://doi.org/10.1016/j.jcis.2006.04.049

Yang Z, Peng XF, Chu CP et al (2006) Sedimentation of Permeable Floc Dry Technol 24:1277–1282. https://doi.org/10.1080/07373930600840393

Ye L, Manning AJ, Hsu TJ (2020) Oil-mineral flocculation and settling velocity in saline water. Water Res 173:115569. https://doi.org/10.1016/j.watres.2020.115569

Ye L, Manning AJ, Hsu TJ et al (2018) Novel application of laboratory instrumentation characterizes mass settling dynamics of oil-mineral aggregates (OMAs) and oil-mineral-microbial interactions. Mar Technol Soc J 52:87–90. https://doi.org/10.4031/MTSJ.52.6.14

Zhang J, Li F, Lv Q et al (2021) Impact of the water–sediment regulation scheme on the phytoplankton community in the Yellow River estuary. J Clean Prod 294:126291. https://doi.org/10.1016/j.jclepro.2021.126291

Zhang J, Zhang Q (2015) Direct simulation of drag force on fractal flocs during settling. J Coast Res 753–757. https://doi.org/10.2112/SI73-129.1

Zhang N, Thompson CEL, Townend IH et al (2018) Nondestructive 3D imaging and quantification of hydrated biofilm-sediment aggregates using X-ray Microcomputed Tomography. Environ Sci Technol 52:13306–13313. https://doi.org/10.1021/acs.est.8b03997

Zhao JX, Yang GL, Kreitmair M, Yue Y (2018) A simple method for calculating in-situ settling velocities of cohesive sediment without fractal dimensions. J Zhejiang Univ Sci A 19:544–556. https://doi.org/10.1631/jzus.A1700185

Zhu Z (2019) A formula for the settling velocity of cohesive sediment flocs in water. Water Sci Technol Water Supply 19:1422–1428. https://doi.org/10.2166/ws.2019.007

Zhu Z, Peng D, Dou J (2018) Changes in the two-dimensional and perimeter-based fractal dimensions of kaolinite flocs during flocculation: a simple experimental study. Water Sci Technol 77:861–870. https://doi.org/10.2166/wst.2017.603